Volume 9 | Number 44 | 28 November 2017 | Pages 17149–17624

Nanoscale

rsc.li/nanoscale

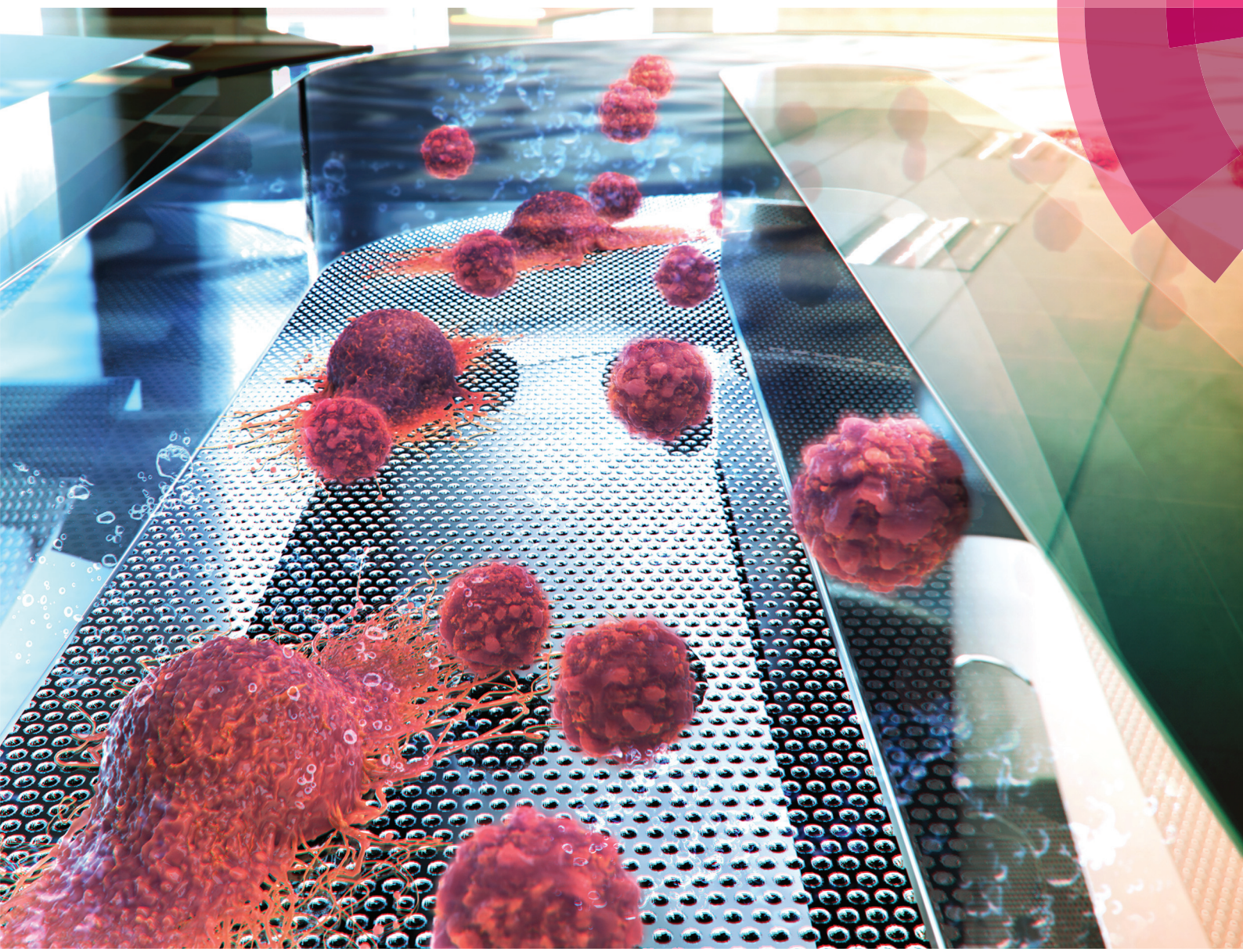

ISSN 2040-3372

ROYAL SOCIETY OF CHEMISTRY

PAPER
Sang-Kwon Lee *et al.*
Microfluidic channel-coupled 3D quartz nanohole arrays for high capture and release efficiency of BT20 cancer cells

NCNST

Nanoscale

PAPER

View Article Online
View Journal | View Issue

Cite this: *Nanoscale*, 2017, **9**, 17224

Microfluidic channel-coupled 3D quartz nanohole arrays for high capture and release efficiency of BT20 cancer cells†

Jung-Taek Lim, [a] Yo-Seop Yoon, [a] Won-Yong Lee, [a] Jin-Tak Jeong, [a] Gil-Sung Kim, [a] Tae Geun Kim [b] and Sang-Kwon Lee *[a]

Nanostructured materials, such as silicon nanowires, quartz nanostructures, and polymer-modified nanostructures, are a promising new class of materials for the capture and enumeration of very rare tumor cells, including circulating tumor cells (CTCs), to examine their biological characteristics in whole blood of cancer patients. These cells can then be used for transplantation, anti-tumor cell therapy, and cell-secreted protein studies. It is believed that 3-dimensional (3D) nanostructured substrates efficiently enhance cell capture yields due to the increased local contacts between the 3D nanostructures and extracellular extensions of the tumor cells. Recent studies have been performed with enhanced cell capture yields thanks to various nanostructured platforms; however, there remains an urgent need both to capture and release viable rare tumor cells for further molecular (*i.e.*, protein) analysis and to develop patient-specific drugs. Here, we first demonstrate that our 3D quartz nanohole array (QNHA) tumor cell capture and release system allows us not only to selectively capture rare tumor cells, but also to release the cells with high capture and release rates. This system was developed using streptavidin (STR)-functionalized QNHA (STR-QNHA) with a microfluidic channel. Our system has ideal cell-separation yields of as high as 85–91% and high release rates of >90% for the BT20 cell line. We suggest that the use of a microfluidic channel technique coupled with a STR-QNHA cell capture and release chip (STR-QNHA cell chip) would be a powerful and simple process to evaluate the capture, enumeration, and release of CTCs from patient whole blood for studying further cell therapy and tumor-cell-secreted molecules.

Received 9th July 2017,
Accepted 1st October 2017

DOI: 10.1039/c7nr04961g

rsc.li/nanoscale

Introduction

Circulating tumor cells (CTCs) are cancer cells that originally propagate from tumors or metastatic sites, spreading into the bloodstream as the cellular origin of fatal metastasis.[1] It has been reported that cancer metastasis can be detected by quantitating these CTCs from patient whole blood.[2,3] Recently, significant progress has been made in rare CTC capture and subsequent enumeration with various nanostructured materials, including silicon nanowires, quartz nanorods, and polymer- and aptamer-modified nanostructures as cell capture platforms.[4–8] It is believed that 3-dimensional (3D) nanostructure substrates efficiently enhance cell capture yields due to the increased local contacts between the 3D nanostructures and extracellular extensions. CellSearch® is the only Food and Drug Administration (FDA)-approved system and is known as the "gold standard" among the emerging CTC capture and isolation methods.[9] In addition, microfluidic-based methods have provided a new approach to capture and count CTCs using various novel structures.[10–13] However, these techniques are generally limited to identify and further characterize the CTCs due to the extremely low number of CTCs present in blood (1–100 CTCs per ml).[3,14,15] Recently, we have developed nanostructure-based platforms, including silicon nanostructures, quartz nanopillars, and quartz nanoholes, for the capture and enumeration of specifically targeted cells from both a cell line and a patient's whole blood. We have proposed that these nanostructure platforms can significantly improve cell capture efficiency (>93%) due to their 3D nano-topographic feature of enhancing local contacts with the cellular surface of tumor cells and their cell capture.[16–18]

Using a set of quartz nanohole arrays (QNHA) with varying hole and pitch sizes, we found that our mechanistic study on nanostructure-based immune cell capture provided new insights into not only the biology of cell–nanomaterial interaction, but also the design of new rare cell capture techno-

[a]*Department of Physics, Chung-Ang University, Seoul 06974, Republic of Korea. E-mail: sangkwonlee@cau.ac.kr*
[b]*School of Electrical Engineering, Korea University, Seoul 02841, Republic of Korea*
†Electronic supplementary information (ESI) available. See DOI: 10.1039/c7nr04961g

logies with improved efficiency and specificity. The majority of recent studies have focused on enhancing cell capture efficiency with various nanostructure platforms. However, a new platform that enables cell capture and release at high yield is strongly required for further investigation of secreted biomolecules (*i.e.*, tumor markers or specific proteins) from captured CTCs to provide more valuable insight into rare tumor cell biology.

Here, we first demonstrate streptavidin-functionalized 3D quartz nanohole arrays (STR-QNHA cell chip) combined with a microfluidic system that enables the selective capture of rare tumor cells and their subsequent release at high yield. This platform uses STR–biotin conjugation in order to allow higher affinity binding with rare tumor cells than the conventional antigen–antibody conjugation, which in turn led to excellent cell capture yields of 85–90% and high release rates of >91% when using the BT20 cell line. Furthermore, our STR-QNHA platform has the advantage of being transparent, which will facilitate further research using fluorescence microscopes compared to previous opaque silicon nanostructure-based platforms.[7,8]

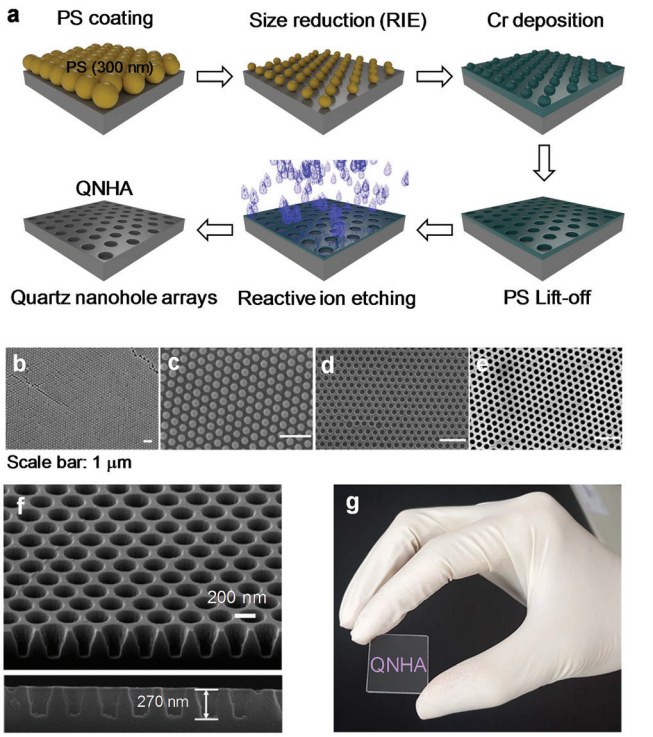

Fig. 1 Fabrication of quartz nanohole arrays (QNHA) using a modified self-assembly technique. (a) Schematic diagram of the QNHA fabrication process: (1) 300 nm polystyrene (PS) nanoparticle coating on a quartz substrate (2.5 × 2.5 cm^2); (2) O_2 plasma etching of PS to produce a space between the PS nanoparticles; (3) 25 nm thick Cr metal deposition using an e-beam evaporator; (4) lift-off process; (5) RIE process for dry etching of the quartz substrate using a Cr metal etch mask; (6) removal of the Cr metal. (b)–(e) FE-SEM images of each fabrication process, including (b) PS coating, (c) RIE etching for space, (d) RIE and PS removal, and (e) removal of Cr metal on QNHA substrates. (f) Tilt and cross-sectional FE-SEM images of the prepared QNHA substrate. (g) Photograph of the QNHA substrate.

Experimental details

QNHA fabrication and surface functionalization

Fig. 1a reveals the typical modified self-assembly technique we developed previously to generate the QNHA using colloidal polystyrene (PS) nanoparticles.[16,18,19] Briefly, the monolayer of colloidal PS nanoparticles of ~300 nm in diameter was first coated on a quartz substrate (2.5 × 2.5 cm^2) (Fig. 1b). The coated PS particles underwent O_2 plasma etching for 45 s (O_2/Ar = 35/10 sccm, RF power of 100 W, and bias power of 50 W) to produce a space between the coated PS nanoparticles (Fig. 1c) followed by 25 nm thick Cr deposition *via* e-beam evaporation as an etch-mask. The reactive ion etching (RIE) process was then performed for 4 min (CF_4/O_2 = 45/5 sccm, RF power of 150 W, and bias power of 50 W). Subsequently, the PS nanoparticles on the quartz substrate were removed by ultrasonication in *N*-methyl-2-pyrrolidone (Fig. 1d). The Cr metal layer was completely removed *via* a lift-off process using the Cr etchant (CR-7, Cyantek, USA) as shown in Fig. 1e. The tilted and cross-sectional views of field-effect scanning electron microscopy (FE-SEM) and the photograph of bare QNHA with a diameter and a depth of ~270 nm are shown in Fig. 1f and g, respectively, revealing that the nanohole arrays are evenly fabricated on the quartz substrates.

Fig. 2a shows the typical STR-surface functionalization of QNHA substrates. For the STR-functionalization of QNHA (Fig. 1a), the QNHA substrates were first cleaned with $H_2O_2 : H_2SO_4$ (1 : 1) for 10 min to remove organic impurities on the surface. Next, the substrates were washed using a three-step cleaning process (acetone, isopropyl alcohol, and distilled water), and then air dried. The QNHA surface was exposed to O_2 plasma for 20 s to immobilize the hydroxyl groups on the QNHA surface for 10 min. The surface underwent a three-step surface functionalization process using 1% (v/v) (3-aminopropyl)-triethoxysilane (APTES, Sigma-Aldrich, USA) in ethanol for 30 min at 23 °C, 12.5% (v/v) glutaraldehyde (GA, Sigma-Aldrich, USA) in distilled water for 4 h on a 3D-rocker, and 50 μg ml^{-1} streptavidin (STR, Sigma-Aldrich, USA) solution in phosphate buffered saline (PBS, Sigma-Aldrich, USA) in an incubator (37 °C, 5% CO_2) overnight. As shown in Fig. 2b, a microfluidic channel was prepared in a conventional polydimethylsiloxane (PDMS, 2.5 × 2.5 cm^2) chamber, a widely used silicon elastomer for bio-microfluidics.[20] Sylgard 184 PDMS pre-polymer was mixed with a curing agent at a volume ratio of 10 : 1, poured onto the salinized silicon wafer containing channel patterns (height of 100 μm and width ranging from 100 to 1000 μm) by photo-lithography and a deep dry etching process, degassed for 30 min, and then cured at 80 °C for 1 h. The PDMS channels were prepared with four types of channels (100, 250, 500, and 1000 μm in width) to examine optimized channel design for microfluidic-based cell chips. This PDMS channel chamber (top image of Fig. 2b) was bound onto an

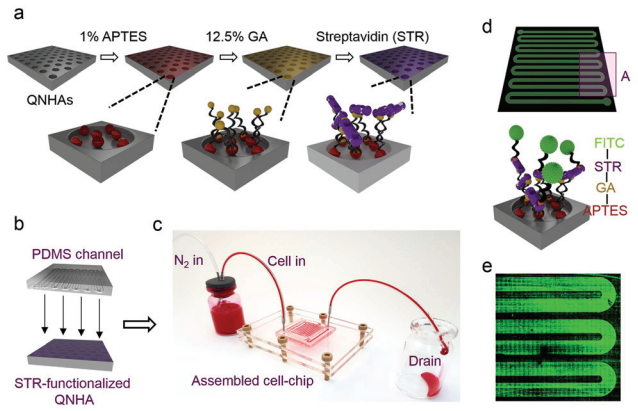

Fig. 2 Surface functionalization of the fabricated QNHA substrates. (a) Surface functionalization of QNHA substrates: (1) the formation of amine groups on the surface of the O_2 plasma-treated QNHA substrates with a 1% APTES solution; (2) immobilization of the aldehyde group on APTES-coated QNHA substrates; and (3) immobilization of STR on GA-conjugated QNHA substrates. (b) Schematic image of the assembly of a PDMS microfluidic chamber with an STR-functionalized QNHA cell capture/release chip. (c) Photograph of the assembled STR-QNHA cell capture/release chip, where a red ink was used to facilitate visualization of the system. (d) Schematic illustration, including the corresponding biomolecular configuration, of the surface of the FITC-labeled STR-QNHA cell chip. (e) Enlarged fluorescence image obtained from part A of (d).

STR-functionalized QNHA cell chip (STR-QNHA) to complete the assembly of a microfluidic channel-coupled cell capture/release chip. Finally, the assembled STR-QNHA cell chip was bound with a plastic plate (Fig. 2c). For the cell capture and release experiments, the assay cell chip was assembled with an N_2 loading system as shown in Fig. 2c and Fig. S1.†

Cell preparation and quantification of captured cells on the STR-QNHA cell chip

For cell capture and release experiments with the STR-immobilized QNHA cell chip, BT20 cells were purchased from American Type Culture Collection (ATCC, USA). Before loading the BT20 cells onto the STR-QNHA cell chip, the BT20 cells were pre-stained using Vybrant cell labeling solution (DiI, 532 nm, Invitrogen, USA) to quantify the captured cells on the STR-QNHA cell chip. DiI-stained BT20 cells were first pre-treated with a biotinylated anti-epithelial cellular adhesion molecule antibody (anti-EpCAM) (Bioscience Inc., USA), a universal biomarker for epithelial tumor cells, and then stored at 4 °C for 20 min.[12] To load the BT20 cells onto the STR-QNHA cell chip, the BT20 cells were manually counted using a conventional hemocytometer (Hausser Scientific Co., USA) with a 10% margin of error, and cell populations were diluted to ~5000 cells per ml in 1× PBS solution. The cell suspension (total volume of 1 ml) was loaded into the four STR-QNHA cell chip types (100, 250, 500, and 1000 μm in width) using an N_2 loading system (Fig. S1†), where the flow rates (0.5 to 4 ml h^{-1}) were controlled by applying N_2 pressure (Fig. S1†). The actual flow rates were determined by measuring the amount of 1× PBS solution at the outlet of the STR-QNHA cell chip for 1 h under a different N_2 pressure (Fig. S1†).

After cell capture experiments with the STR-QNHA cell chip, the captured cells were washed using 1× PBS solution at least five times to remove unbound tumor cells. BT20 cells bound on the STR-QNHA cell chip were then fixed with 4% paraformaldehyde (PFA, Santa Cruz Biotechnology Inc., USA) in PBS for 20 min, followed by washes using PBS after removing the PDMS microfluidic chamber. To quantify the captured BT20 cells on the cell chips, we conducted laser scanning cytometry (LSC), which has been shown to be a useful method,[21] using an Axon Genepix microarray scanner 4000B (Molecular Devices, USA). The QNHA substrate-bound BT20 cells were scanned using a YAG laser (532 nm wavelength) on the microarray scanner with 5 μm resolution. Subsequently, the scanned fluorescence images were transferred into CellProfiler™ analysis software for the quantification of QNHA chip-bound cells.

Results and discussion

Cell capture performance using the STR-immobilized cell chip

To verify that STR proteins were homogenously immobilized on the microfluidic-based QNHA cell chip, the surface of the GA-conjugated QNHA was stained with streptavidin–fluorescein isothiocyanate conjugate (STR-FITC, eBioscience Inc., USA) solution in an incubator for 24 h and then fixed with 4% PFA solution. Fig. 2d shows the schematic illustration of the FITC-labeled STR-QNHA cell chip along with the corresponding biomolecular configuration. Using a microarray scanner, as shown in Fig. 2e, an enlarged fluorescence-activated image was obtained from part A of Fig. 2d. These results clearly demonstrate that the functionalized STR proteins are homogenously immobilized on the surface of the QNHA, leading to uniform fluorescence brightness in a large area of the microfluidic channel in the QNHA cell chip. This indicates that our STR-QNHA cell chip is suitable for fluorescence detection of rare CTCs.

Furthermore, to assess cell integrity on the STR-QNHA cell chip, the surface-bound BT20 cell nuclei were stained with 4′-6-diamidino-2 phenylindole (DAPI, Thermo Fisher Scientific, USA). Fig. 3a–c show the fluorescence images of the DAPI-stained and Dil-stained cells, and the merged fluorescence images of the surface-bound BT20 cells on the STR-QNHA cell chip, respectively. As shown in Fig. 3a–c, the stained cells were subsequently evaluated for the number of BT20 cells (Dil^+/$DAPI^+$) out of the total counted cells bound on the STR-QNHA cell chip by fluorescence microscopy analysis (EVOS™, AMG, USA). Our results indicate that more than 98% of the fluorescence-activated spots on the STR-immobilized QNHA cell chip were identified as the captured BT20 cells (n = 3).

Prior to the cell capture experiments, we prepared four QNHA cell chips with widths of 100, 250, 500, and 1000 μm in PDMS microfluidic channels with a fixed flow rate of 0.5 ml h^{-1} to determine the optimal size of the microfluidic channel. Approximately 5000 BT20 cells per ml were loaded

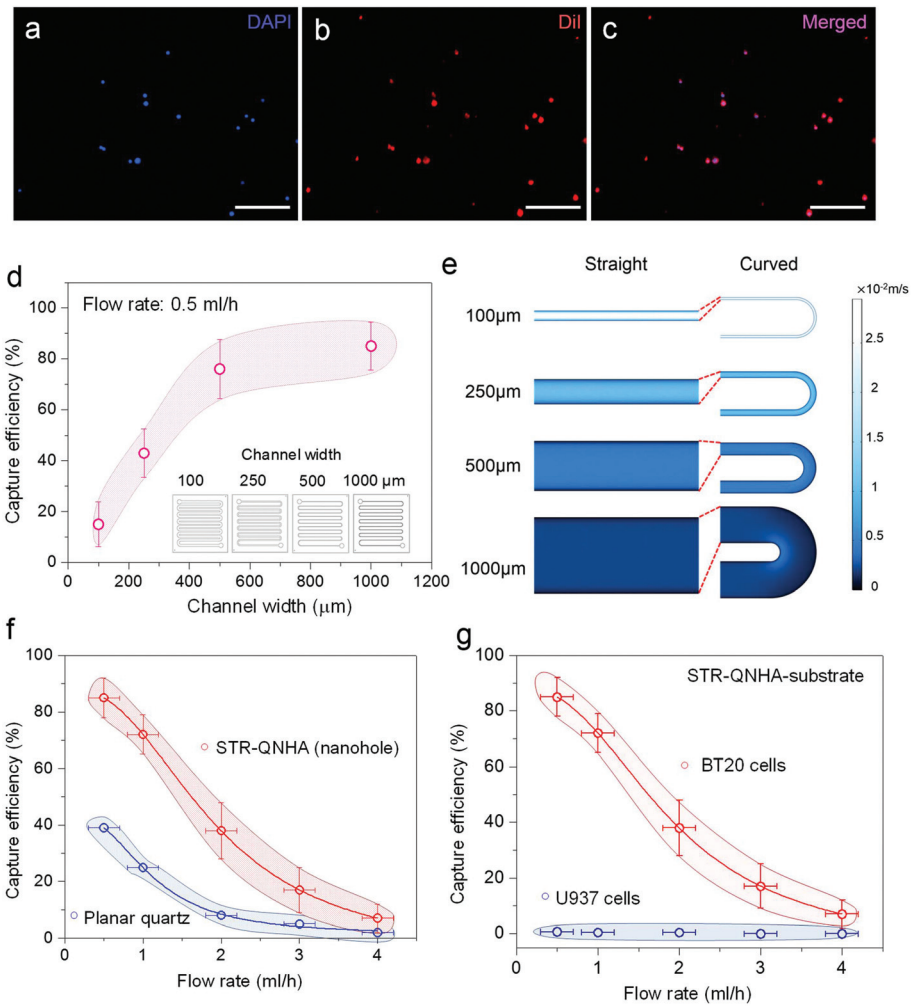

Fig. 3 Cell capture performance using an STR-immobilized QNHA cell chip. (a) Fluorescence images of substrate-bound BT20 cells stained with (a) DAPI, (b) DiI, and (c) merged on the STR-immobilized QNHA cell chip. Scale bar is 200 μm. (d) Average cell capture efficiency (%) of surface-bound BT20 cells for different widths of 100, 250, 500, and 1000 μm at a fixed flow rate of 0.5 ml h^{-1} on the STR-functionalized QNHA cell chip. (e) Fluid-speed distribution of the PDMS microfluidic channel at different zones (straight and curved areas) for different channel widths using the COMSOL simulator. (f) Average cell capture efficiency of surface-bound BT20 cells with two different STR-functionalized cell capture platforms; such as planar quartz substrates (STR-planar quartz cell chip) and an STR-QNHA cell chip, and (g) two different cells (EpCAM-negative U937 monocytes and EpCAM-positive BT20 cells) as a function of flow rate up to 4 ml h^{-1}.

into the STR-QNHA cell chip, and the substrate-bound cells were quantified by LSC imaging (Fig. S2†). As shown in Fig. 3a–c, all loaded BT20 cells were pre-stained with DiI to easily quantify the exact number of the cells in the STR-QNHA cell chip. Fig. 3d shows the cell capture efficiency for different widths of the microfluidic channels ranging from 100 to 1000 μm. When the width of the microfluidic channels are wider than 500 μm, the cell capture efficiency linearly increases from ~15 ± 8.7% (100 μm wide channel) to ~76 ± 11.6%, and then slightly increases again up to ~91%, which is consistent with our previous results using other 3D cell capture platforms[3,18,22] for the 1000 μm wide QNHA cell chip (Fig. 3d). To further investigate the effect of the channel width on the cell capture efficiency of STR-immobilized QNHA cell chips, a commercial multi-physics finite-element solver (COMSOL software, http://www.comsol.com/) was used to simulate the fluid-speed distribution dependent on the channel widths of 100, 250, 500, and 1000 μm in the microfluidic-based STR-QNHA cell chips in a steady-state with a flow rate of 0.5 ml h^{-1}. According to the numerical simulation results using COMSOL (Fig. 3e), the flow rate (*i.e.*, fluid speed) is gradually decreased with increasing the channel width up to 1000 μm. This countertrend, compared to the increased cell capture efficiency (Fig. 3d), is due to the increased probability of contact between the BT20 cells and the STR-bound substrates at a slower flow rate. Based on these results, we determined the optimized width of microfluidic channels for the STR-QNHA cell chip to be 1000 μm. Accordingly, we used the 1000 μm wide channel STR-QNHA cell chip for subsequent experiments.

To quantify the cell capture efficiency of the optimized STR-QNHA cell chip, we conducted cell capture yield experi-

ments at flow rates of 0.5, 1, 2, 3, and 4 ml h^{-1} with a fixed channel width of 1000 μm, where we loaded ~5000 cells per ml into the STR-QNHA cell chip. For comparison, the STR-functionalized planar quartz substrates were also tested as a control sample. Fig. 3f shows the cell capture efficiencies for two-different cell capture platforms (*i.e.*, STR-planar quartz and STR-QNHA cell chip) as a function of flow rates up to 4 ml h^{-1}. These results show that the STR-QNHA cell chip can efficiently capture cells (as high as ~91%, a factor of ~2.3) as compared to the control samples (~39%), which is consistent with previous results.[18,23] The high cell capture efficiency of the STR-QNHA cell chip, compared to the STR-planar quartz substrate, can be explained by an increase in the local contact area between the cells and the solid surface, and 3D surface accessibility, as demonstrated by the FE-SEM image of tightly bound BT20 cells on STR-immobilized QNHA cell chips shown in Fig. S3.† [18] This allows enhanced cell adhesion on the surface of the STR-QNHA substrate compared to the STR-planar substrate, thereby increasing the cell capture efficiency as previously demonstrated.[18] Furthermore, the cell capture efficiency of the STR-QNHA cell chip decreased significantly to ~7 ± 5% upon increasing the flow rate up to 4 ml h^{-1}, whereas the capture efficiency for the control sample decreased slightly to ~2% (Fig. 3f). The reduced cell capture efficiency at higher flow rates could be due to the reduced contact-probability of the BT20 cells to STR-QNHA substrates in the microfluidic channel and increased drag force as seen in previous reports.[5] As a result, the optimized flow rate at a fixed width of 1000 μm in the STR-QNHA cell chip was determined to be ~0.5 ml h^{-1}.

To test the ability to capture specific cells (*i.e.*, anti-EpCAM sensitive and positive tumor cells, BT20), we loaded U937 monocytes (anti-EpCAM-negative cells) into STR-QNHA cell chips under the same experimental conditions. In Fig. 3g, the cell capture efficiency with EpCAM-negative monocytes (U937) was as high as ~0.7% with different flow rates of 0.5 to 4 ml h^{-1}, indicating that our STR-QNHA cell chip for specific tumor cell separation is a promising platform for capturing specific tumor cells (*i.e.*, anti-EpCAM-positive cells), even in metastatic cancer patients in clinical analysis. Our results led us to believe that the optimal cell capture condition—1000 μm wide microchannel with 0.5 ml h^{-1} of flow rate of the QNHA cell chip—was found for cell capture performance studies on EpCAM-positive cell lines.

To further confirm the flow rate dependence on the cell capture efficiency of the STR-immobilized QNHA cell chip, we conducted the numerical simulation for the fluid-speed distribution with flow rates of ~0.5, 1, and 4 ml h^{-1} in the microfluidic channel of the STR-QNHA cell chip in a steady-state. The numerical simulation results using COMSOL visually demonstrate that there is strong flow rate and zone dependence for different fluid speeds (Fig. 4a). Our results suggest that increased fluid speed decreases the probability of reducing cell capture efficiency (Fig. 3f). Thus, the COMSOL results confirm the flow-rate dependence of cell capture efficiency (Fig. 3f and g). As shown in Fig. 4a, the fluid speed passes rapidly from the inside of the curved zone and side area of the straight zone in the PDMS microfluidic channel, which is further discussed in the next section.

To gain an in-depth understanding of the effect of the nano-topological structure on the cell capture efficiency of the STR-immobilized QNHA, we also carried out the numerical COMSOL simulation for the flowing behavior on the solid–fluid interface in the microfluidic channel (~1000 μm in width) of the STR-QNHA cell chip in steady-states with a fixed flow rate of 0.5 ml h^{-1}. For comparison, the STR-functionalized planar quartz substrates were also simulated as a control sample. Fig. 4b shows the numerically calculated flow-speed profiles for the STR-planar (virtual region of A–B) and STR-QNHA (virtual region of A′–B′) at the straight zone in the microchannel, indicating similar flow-speed profiles in both microchannels. According to microscopy COMSOL simulation, the STR-planar microchannel gave rise to a homogeneous laminar flow on the solid–fluid interface (top images of Fig. 4c and d, interfacial region of B–D). On the other hand, the STR-QNHA microchannel shows an inhomogeneous flow distribution due to faster fluid-speed on nanoholes than on the adjacent flat-surface (bottom image of Fig. 4c, marked area C′), which in turn led to turbulent flowing behavior on the nanostructure–fluid interface up to 250 nm-height (bottom image of Fig. 4d, interfacial region of B′–D′). These COMSOL results strongly demonstrate that the high cell capture efficiency of the STR-QNHA cell chip compared to the STR-planar quartz substrate can be attributed to the increased contact-probability and 3D surface-accessibility of the BT20 cells to STR-QNHA substrates, which is induced by an inhomogeneous turbulent flow on the nanohole–fluid interface.

Spatial distribution of substrate-bound BT20 cells in the STR-QNHA cell chip

To test the way in which the spatial orientation of the substrate-bound BT20 cells in microfluidic channels affects the cell capture efficiency of the STR-QNHA cell chip, we performed cell capture experiments at flow rates of 0.5, 1, 2, 3, and 4 ml h^{-1} with a microfluidic channel width of 1000 μm (Fig. 5a and b). The microchannels were marked from zones 1 to 13 (Fig. 5b). After fixing the substrate-bound BT20 cells in the STR-QNHA cell chip, we obtained the fluorescence images of each zone in the microfluidic channels using EVOS™ fluorescence microscopy (Fig. 5c and Fig. S2†). Fig. 5d shows the spatial distribution of the substrate-immobilized BT20 cells in the STR-QNHA cell chip as a function of zone number from 1 to 13 at flow rates of 0.5, 1, 2, 3, and 4 ml h^{-1}. At a flow rate of 0.5 ml h^{-1}, more than 70% of the BT20 cells were bound in approximately the first half of the zones of the STR-QNHA cell chip (Fig. 5d). This is in agreement with previous studies.[5] In the subsequent zones, the substrate-bound BT20 cells were evenly distributed along the microfluidic channels with lower cell capture efficiencies (Fig. 5d). The main reason for the surface-bound cells being distributed in the first few zones of the chip (first image of Fig. 5d) is that there is a high probability that the flowing cells will encounter the STR-QNHA substrates at a low flow rate (~0.5 ml h^{-1}), as discussed previously.

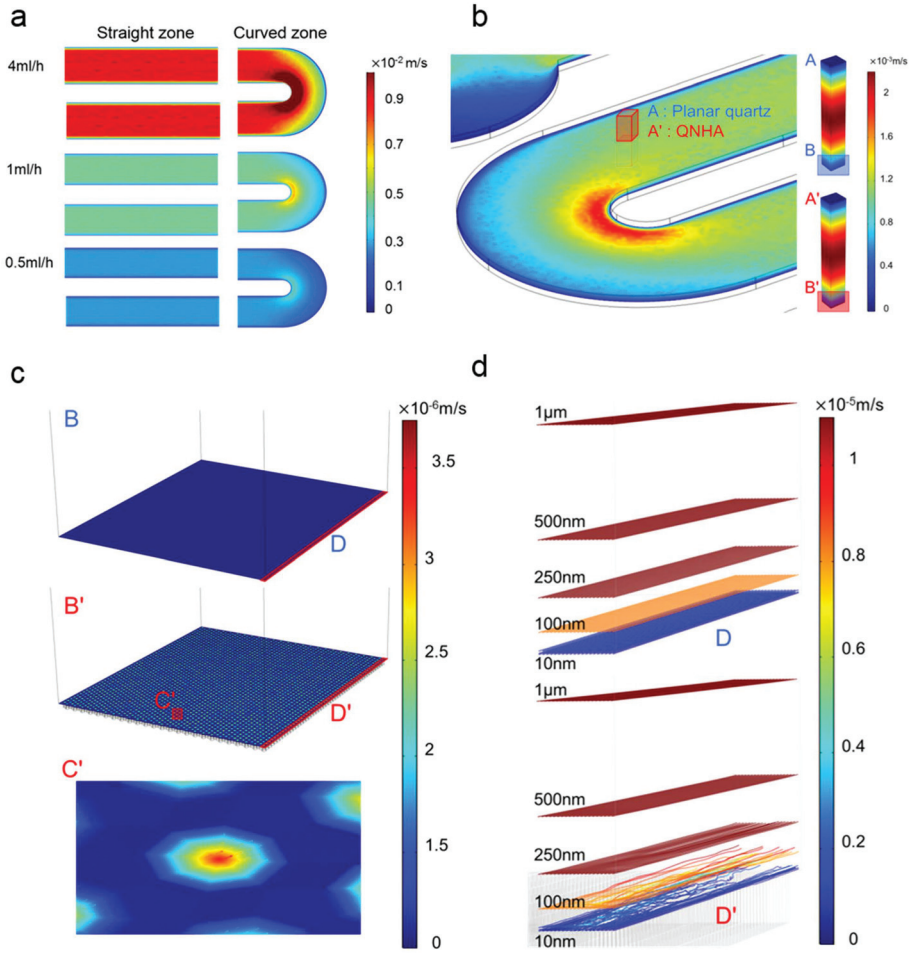

Fig. 4 Numerical COMSOL simulation of the STR-QNHA cell chip. (a) Fluid-speed distribution of the PDMS microfluidic channel (~1000 μm in width) in different zones (straight and curved areas) for different flow rates. (b) Calculated flow-speed profiles for the STR-planar and STR-QNHA in the straight zone of the microfluidic channel with a fixed flow rate of 0.5 ml h^{-1}. (c) Fluid-speed distributions and (d) flow behaviors on the solid–liquid interface (up to 1 μm-height) in the microfluidic channels of STR-planar and STR-QNHA cell chips.

With increasing flow rate (*i.e.*, fluid speed) in the microfluidic channel, there is a reduced probability of contact between the BT20 cells with STR-QNHA substrates, which in turn can result in a reduction in both the cell distribution in the zone and the overall cell capture efficiency (Fig. 5d).

To identify the area of the microfluidic channels where the substrate-bound BT20 cells are located, we obtained fluorescence images at the straight and curved zones, as shown in Fig. 5e (at a flow rate of 0.5 ml h^{-1}) and Fig. S4† (at a flow rate of 4 ml h^{-1}). Most of the substrate-bound cells were found inside the straight microfluidic channel and outside the curved microfluidic channel (Fig. 5e and Fig. S4†), implying that cell capture efficiency is dependent on the position within the microfluidic channel at flow rates of 0.5 and 4 ml h^{-1}. There were two common data points in terms of cell capture position between the straight and curved area of the microfluidic channels; however, overall, the cell capture efficiency at 4 ml h^{-1} is much lower than at 0.5 ml h^{-1}. This observation can be explained by laminar flow in circular pipes (*i.e.*, microfluidic channel), in which the layers of liquid flow in a uniform fashion and generally have a parabolic flow profile.[24] Furthermore, the substrate-bound cells were stained with DAPI to identify the cells as shown in Fig. 5e (top and bottom areas of the three images on the right) and Fig. S4.† We found that the majority of fluorescence spots were identified as substrate-bound BT20 cells (>98%).

To further support the observations depicted in Fig. 5e, we used a multi-physics finite-element solver (COMSOL) for the fluidic simulation in the microfluidic channel (Fig. 5f–h) in a steady-state. In the simulation, the geometry of the microchannel (Fig. 5f) was defined exactly to match the size of the PDMS microfluidic channel. Fig. 5g and h show the numerically calculated virtual images of the flow-speed profiles at the curved areas of the microchannel with a cross-sectional profile (bottom images of Fig. 4h) at a flow rate of 0.5 ml h^{-1}. As shown in Fig. 5g, the fluid speed inside is much faster (>a factor of 4) than the outside of the microfluidic channel. These results further demonstrate that increased fluid-speed reduces the probability of contact between the cells and the STR-bound substrates, which in turn reduces the cell capture efficiency in that area.

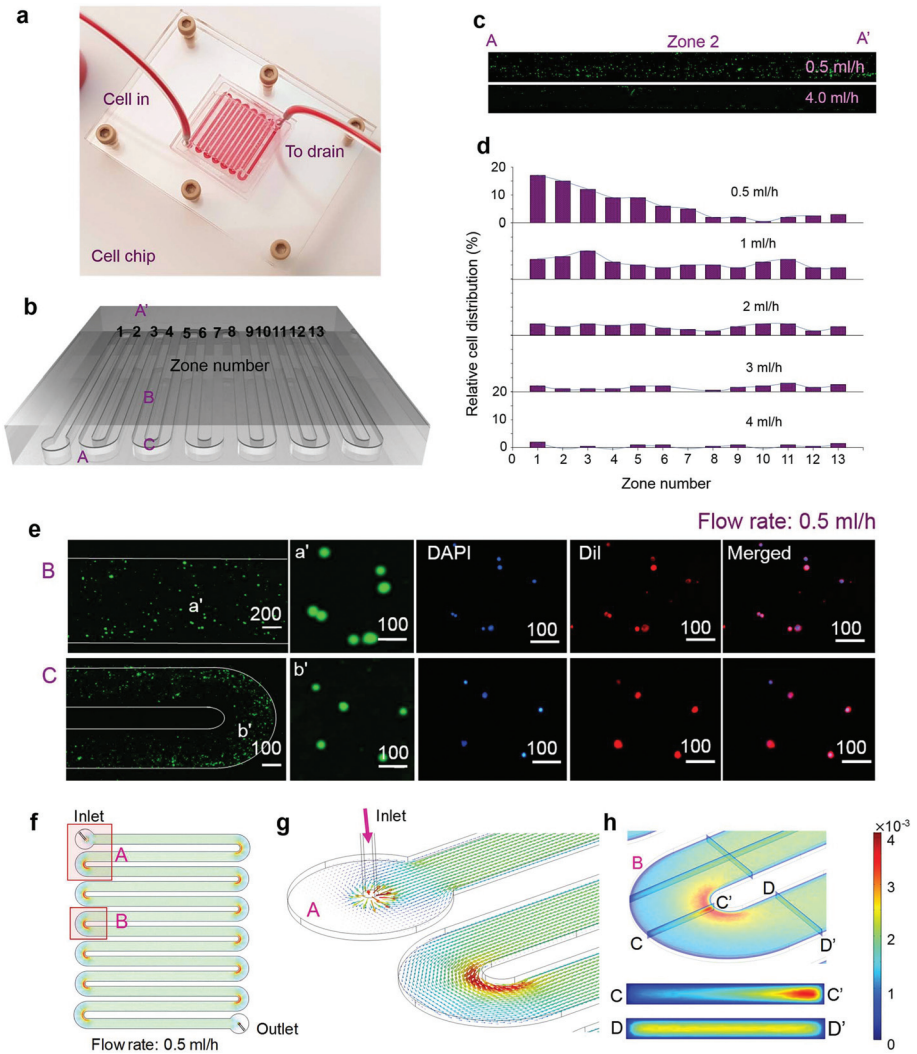

Fig. 5 Spatial distribution of substrate-bound BT20 cells in the STR-QNHA cell chip. (a) Photograph of the STR-functionalized QNHA cell chip. (b) PDMS-based microfluidic channel marking zones 1 to 13. (c) Fluorescence image of substrate-bound BT20 cells in the STR-QNHA cell chip for flow rates of 0.5 and 4.0 ml h^{-1} along A–A′ in zone 2 in (b). (d) Substrate-bound cell distribution of the STR-QNHA cell capture chip as a function of zone number and flow rates up to 4 ml h^{-1}. (e) Fluorescence images (*i.e.*, laser-scanned DiI, DAPI, DiI, and merged) of substrate-bound BT20 cells stained on the STR-QNHA cell chip at marked areas B and C as in (b) at a flow rate of 0.5 ml h^{-1}. (f) Numerically calculated virtual image of flow speed in the PDMS microfluidic channel using a commercial COMSOL simulator. (g), (h) Enlarged images of the flow direction (A) and cross-sectional images along C–C′ and D–D′ of fluid speed in the curved area, respectively.

Cell release efficiency using a microfluidic-based cell chip

The cell release efficiency was tested by placing the BT20-captured STR-QNHA cell chips in an incubator at 37 °C for 5 min with trypsin. In particular, the BT20-captured STR-QNHA cell chips were obtained using the same protocol as the cell capture experiments: ~5000 cells per ml were initially loaded into the STR-immobilized QNHA cell chip at a flow rate of 0.5 ml h^{-1}. All the chips were then washed out at least three times with PBS after removing the PDMS microfluidic chamber. To break cell-to-substrate connections, ~1 ml of diluted 0.25% trypsin solution (Invitrogen, USA) was loaded onto the BT20-captured STR-QNHA cell chips, followed by a 5 min wait to detach the cells in an incubator at 37 °C. After finishing trypsinization, the STR-QNHA cell chips were washed using 1× PBS solution at least five times to neutralize the trypsin. The remaining BT20 cells on the STR-QNHA cell chip were fixed and enumerated again using a microarray scanner, followed by CellProfiler™ analysis as conducted in the cell capture assays. Fig. 6a and b show the fluorescence images of the surface-bound BT20 cells in the first two microfluidic channels (zones 1 and 2 in Fig. 5b). As shown in Fig. 6c, approximately 90.7 ± 1.4% of the substrate-immobilized BT20 cells are released from the surface of the STR-immobilized QNHA cell chip after a 5 min treatment with trypsin. These results demonstrate desirable cell-release performance and are consistent with previous reports.[8,25,26] In contrast to the protruded nanostructures, including silicon nanowires, the 3D

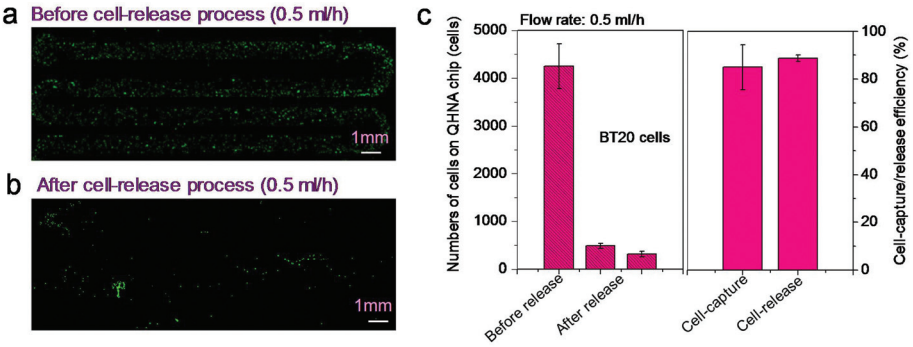

Fig. 6 Cell release performance of the STR-immobilized QNHA cell chip. Enlarged fluorescence images of substrate-bound BT20 cells in a specific area (a) before and (b) after the cell-release process at a flow rate of 0.5 ml h^{-1}, respectively. The cell release process was performed with 5 min trypsin treatment. (c) Cell release performance of the STR-functionalized QNHA cell chip.

and smooth QNHA structures allowed us to efficiently capture and release the cells; however, the protruded nanostructures provided a higher cell capture efficiency with a relatively lower release rate and low viability due to the strong adhesion forces between the cell and the substrates, as described in previous reports.[5,7,22] Furthermore, the trypsinized suspension was neutralized with PBS solution and spun at 1000 rpm for 3 min, followed by the removal of the supernatant and re-suspension of the BT20 cells in ~ 1 ml of the PBS solution. To investigate the viability of the released BT20 cells from the STR-QNHA cell chip, the re-suspended BT20 cells were stained with DAPI (blue color in Fig. S5†) and propidium iodide (PI, Invitrogen, USA, red color in Fig. S5†). The DAPI stains all nuclei of the cells, while PI passes through the cell membrane of dead cells and stains DNA. By enumerating the dead cells (PI^+) out of total cells ($DAPI^+$) using fluorescence microscopy, more than 75% of the released BT20 cells from the STR-QNHA cell chip were viable (Fig. S5e†).

There have been several recent studies regarding cell capture and release platforms in a single chip. Shen *et al.* reported a specific capture and release platform using DNA aptamer-modified silicon nanowires, where enzyme-induced cell-release studies were conducted.[8] From their reports we found that more than 90% of substrate-immobilized cells were specifically released in an enzyme incubation time-dependent manner. Similar results have recently been published by Hou *et al.* in 2013.[7] For cell capture/release efficiency, they used polymer-grafted silicon nanowires, which can be temperature sensitive. Although similar studies on cell capture/release performances (>90% cell capture/release efficiency) have been reported and there has been substantial improvement in methods, our STR-immobilized QNHA cell capture/release chips are expected to be very beneficial in the field. Our promising platform, which we believe is reliable, has enhanced cell capture and release efficiency (>90%) on STR-immobilized QNHA cell chips compared to protruding nanostructures, including silicon nanowires and quartz nanorods.[3,19,21] This effect can be explained by the 3D nanostructures of STR-immobilized QNHA cell chips in microfluidic channels, and STR-immobilization on the QNHA surface that enables high affinity binding to biotin-conjugated monoclonal antibodies (K_d = 10^{-15} M) directed against specific cell surface markers. This is in contrast with the conventional antigen–antibody conjugation, as we have previously discussed.[23] Furthermore, our STR-QNHA platform has the advantage of being transparent, which will facilitate further research using fluorescence microscopes compared to previous opaque silicon nanostructure-based platforms.[7,8,27,28] Another important advantage of our STR-QNHA cell chip is that it does not require further functionalization, especially for cell release performance as previous methods require, such as additional polymer-functionalization into silicon nanostructures reported by Hou *et al.*[7] Our STR-QNHA cell chip is simple, highly effective, and highly efficient for both cell capture and cell release assays. On the basis of STR-QNHA cell capture/release performance, our platform can further provide a CTC-secreted molecular signature and functional readout from the released CTCs while causing minimal damage to clinical cancer biology.

Conclusions

In summary, we have demonstrated that 3D STR-immobilized QNHA cell chips can not only selectively capture rare tumor cells, but also release the captured tumor cells with a capture/release efficiency of as high as 90%. This cell capture and release platform combines the STR-immobilized QNHA substrate with a PDMS microfluidic channel. Our results clearly suggest that the use of a microfluidic technique combined with a 3D QNHA platform would be a powerful and appropriate tool for the capture, enumeration, and release of CTCs to further study cell therapy and tumor cell-secreted proteins. This is the first mechanistic study on nanostructure-based CTC cell capture/release performance and provides new insights into not only the biology of cell–nanomaterial interaction but also the design of rare tumor cell capture/release technologies with improved efficiency, specificity, and purity.

Conflicts of interest

There are no conflicts to declare.

Acknowledgements

This study was supported by the Priority Research Centers Program and by the Basic Science Research Program through the National Research Foundation of Korea (NRF) funded by the Ministry of Education, Science, and Technology (2009-0093817, 2015R1A2A1A15055313, and 2016R1A3B1908249).

References

1 B. Mostert, S. Sleijfer, J. A. Foekens and J. W. Gratama, *Cancer Treat. Rev.*, 2009, **35**, 463–474.
2 A. Jain and L. L. Munn, *Lab Chip*, 2011, **11**, 2941–2947.
3 S. K. Lee, G. S. Kim, Y. Wu, D. J. Kim, Y. Lu, M. Kwak, L. Han, J. H. Hyung, J. K. Seol, C. Sander, A. Gonzalez, J. Li and R. Fan, *Nano Lett.*, 2012, **12**, 2697–2704.
4 S. T. Wang, K. Liu, J. Liu, Z. T. F. Yu, X. W. Xu, L. B. Zhao, T. Lee, E. K. Lee, J. Reiss, Y. K. Lee, L. W. K. Chung, J. T. Huang, M. Rettig, D. Seligson, K. N. Duraiswamy, C. K. F. Shen and H. R. Tseng, *Eur. Biophys. J.*, 2011, **40**, 235.
5 S. T. Wang, K. Liu, J. A. Liu, Z. T. F. Yu, X. W. Xu, L. B. Zhao, T. Lee, E. K. Lee, J. Reiss, Y. K. Lee, L. W. K. Chung, J. T. Huang, M. Rettig, D. Seligson, K. N. Duraiswamy, C. K. F. Shen and H. R. Tseng, *Angew. Chem., Int. Ed.*, 2011, **50**, 3084–3088.
6 S. T. Wang, H. Wang, J. Jiao, K. J. Chen, G. E. Owens, K. I. Kamei, J. Sun, D. J. Sherman, C. P. Behrenbruch, H. Wu and H. R. Tseng, *Angew. Chem., Int. Ed.*, 2009, **48**, 8970–8973.
7 S. Hou, H. C. Zhao, L. B. Zhao, Q. L. Shen, K. S. Wei, D. Y. Suh, A. Nakao, M. A. Garcia, M. Song, T. Lee, B. Xiong, S. C. Luo, H. R. Tseng and H. H. Yu, *Adv. Mater.*, 2013, **25**, 1547–1551.
8 Q. L. Shen, L. Xu, L. B. Zhao, D. X. Wu, Y. S. Fan, Y. L. Zhou, W. H. OuYang, X. C. Xu, Z. Zhang, M. Song, T. Lee, M. A. Garcia, B. Xiong, S. Hou, H. R. Tseng and X. H. Fang, *Adv. Mater.*, 2013, **25**, 2368–2373.
9 S. Riethdorf, H. Fritsche, V. Muller, T. Rau, C. Schindibeck, B. Rack, W. Janni, C. Coith, K. Beck, F. Janicke, S. Jackson, T. Gornet, M. Cristofanilli and K. Pantel, *Clin. Cancer Res.*, 2007, **13**, 920–928.
10 J. Schneider, T. Bachmann, D. Franco, P. Richner, P. Galliker, M. K. Tiwari, A. Ferrari and D. Poulikakos, *Macromol. Biosci.*, 2013, **13**, 973–983.
11 P. G. Schiro, M. X. Zhao, J. S. Kuo, K. M. Koehler, D. E. Sabath and D. T. Chiu, *Angew. Chem., Int. Ed.*, 2012, **51**, 4618–4622.
12 S. Nagrath, L. V. Sequist, S. Maheswaran, D. W. Bell, D. Irimia, L. Ulkus, M. R. Smith, E. L. Kwak, S. Digumarthy, A. Muzikansky, P. Ryan, U. J. Balis, R. G. Tompkins, D. A. Haber and M. Toner, *Nature*, 2007, **450**, 1235–U1210.
13 A. A. Adams, P. I. Okagbare, J. Feng, M. L. Hupert, D. Patterson, J. Gottert, R. L. McCarley, D. Nikitopoulos, M. C. Murphy and S. A. Soper, *J. Am. Chem. Soc.*, 2008, **130**, 8633–8641.
14 S. Maheswaran, L. V. Sequist, S. Nagrath, L. Ulkus, B. Brannigan, C. V. Collura, E. Inserra, S. Diederichs, A. J. Iafrate, D. W. Bell, S. Digumarthy, A. Muzikansky, D. Irimia, J. Settleman, R. G. Tompkins, T. J. Lynch, M. Toner and D. A. Haber, *New Engl. J. Med.*, 2008, **359**, 366–377.
15 M. Yu, A. Bardia, B. Wittner, S. L. Stott, M. E. Smas, D. T. Ting, S. J. Isakoff, J. C. Ciciliano, M. N. Wells, A. M. Shah, K. F. Concannon, M. C. Donaldson, L. V. Sequist, E. Brachtel, D. Sgroi, J. Baselga, S. Ramaswamy, M. Toner, D. A. Haber and S. Maheswaran, *Science*, 2013, **339**, 580–584.
16 G. S. Kim, D. J. Kim, J. H. Hyung, M. K. Lee and S. K. Lee, *Anal. Chem.*, 2014, **86**, 5330–5337.
17 K. E. Fischer, B. J. Aleman, S. L. Tao, R. H. Daniels, E. M. Li, M. D. Bunger, G. Nagaraj, P. Singh, A. Zettl and T. A. Desai, *Nano Lett.*, 2009, **9**, 716–720.
18 D. J. Kim, G. S. Kim, J. K. Seol, J. H. Hyung, N. W. Park, M. R. Lee, M. K. Lee, R. Fan and S. K. Lee, *J. Biomed. Nanotechnol.*, 2014, **10**, 1030–1040.
19 D. J. Kim, J. K. Seol, Y. Wu, S. Ji, G. S. Kim, J. H. Hyung, S. Y. Lee, H. Lim, R. Fan and S. K. Lee, *Nanoscale*, 2012, **4**, 2500–2507.
20 M. A. Unger, H. P. Chou, T. Thorsen, A. Scherer and S. R. Quake, *Science*, 2000, **288**, 113–116.
21 J. Zhou, Y. Wu, S. K. Lee and R. Fan, *Lab Chip*, 2012, **12**, 5025–5033.
22 S. K. Lee, D. J. Kim, G. Lee, G. S. Kim, M. Kwak and R. Fan, *Biosens. Bioelectron.*, 2014, **54**, 181–188.
23 S. T. Kim, D. J. Kim, T. J. Kim, D. W. Seo, T. H. Kim, S. Y. Lee, K. Kim, K. M. Lee and S. K. Lee, *Nano Lett.*, 2010, **10**, 2877–2883.
24 T. Kobayashi, T. Funamoto, M. Hosaka and S. Konishi, *Jpn. J. Appl. Phys.*, 2010, **49**, 06GP03.
25 L. Chen, X. L. Liu, B. Su, J. Li, L. Jiang, D. Han and S. T. Wang, *Adv. Mater.*, 2011, **23**, 4376–4380.
26 Y. Wan, Y. L. Liu, P. B. Allen, W. Asghar, M. A. I. Mahmood, J. F. Tan, H. Duhon, Y. T. Kim, A. D. Ellington and S. M. Iqbal, *Lab Chip*, 2012, **12**, 4693–4701.
27 D. J. Kim, M. K. Choi, J. T. Jeong, J. T. Lim, H. B. Lee, W. Han and S. K. Lee, *J. Biomed. Nanotechnol.*, 2016, **12**, 645–655.
28 D. J. Kim, W. Y. Lee, N. W. Park, G. S. Kim, K. M. Lee, J. Kim, M. K. Choi, G. H. Lee, W. Han and S. K. Lee, *Biosens. Bioelectron.*, 2015, **67**, 370–378.

